UFSM

CIÊNCIA e NATURA

ISSN 2179-460X
OPEN ACCESS

Ci. e Nat., Santa Maria, v. 46, spe. n. 1, e87036, 2024 • https://doi.org/10.5902/2179460X87036
Submitted: 09/03/2024 • Approved: 25/06/2024 • Published: 04/11/2024

Special edition ERMAC e ENMC

Influence of aluminum doping on the mechanical properties of bilayer silicene

Influência da dopagem de alumínio nas propriedades mecânicas do siliceno bicamada

Bryan Angel Leite dos Santos[I], Alexandre Melhorance Barboza[I], Luis César Rodríguez Aliaga[I], Ivan Napoleão Bastos[I]

[I] Universidade do Estado do Rio de Janeiro, Nova Friburgo, RJ, Brazil

ABSTRACT

Silicene, a two-dimensional material with potential applications in future technologies, has garnered significant interest in the past decade. Recent attention has focused on modifying silicene's electronic and magnetic properties through adatom adsorption or substitutional doping. While the magnetic, electronic, and optical properties of doped silicene have been extensively studied, a noticeable gap exists in the literature concerning its mechanical properties. In this context, this study addresses this gap by exploring the mechanical characteristics of bilayer silicene doped with aluminum by employing molecular dynamics simulations. The influence of Al concentration on the material's mechanical response is assessed by tensile tests performed at a strain rate of 10^{10} s^{-1}. The findings reveal a monotonically decreasing strength with Al concentration in both loading directions, zigzag and armchair. The deformation initiates with the rupture of Si-Al bonds, ultimately leading to a brittle fracture.

Keywords: Bilayer silicene; Doping; Aluminum; Molecular dynamics; Mechanical properties

RESUMO

O siliceno, um material bidimensional com aplicações potenciais em futuras tecnologias, tem despertado grande interesse na última década. Recentemente, bastante atenção vem sendo dada a modificação das propriedades eletrônicas e magnéticas do siliceno por meio da adsorção de adátomos ou da dopagem substitucional. Enquanto as propriedades magnéticas, eletrônicas e óticas do siliceno dopado foram extensivamente estudadas, existe uma lacuna na literatura em relação às suas propriedades mecânicas. Neste contexto, este estudo aborda essa lacuna explorando as características mecânicas do silicene bilayer dopado com alumínio por meio de simulações de dinâmica molecular. A influência da concentração de Al na resposta mecânica do material é avaliada por testes de tração realizados a uma taxa de deformação de 10^{10} s^{-1}. Os resultados revelam uma diminuição monotônica da resistência

mecânica com a concentração de Al em ambas as direções de carregamento, zigzag e armchair. A deformação se inicia com a ruptura das ligações Si-Al, levando eventualmente a uma fratura frágil.

Palavras-chave: Siliceno bicamada; Dopagem; Alumínio; Dinâmica molecular; Propriedades mecânicas

1 INTRODUCTION

With a structure similar to graphene, silicene consists of a two-dimensional (2D) sheet of silicon atoms arranged in a hexagonal lattice. Its theoretical prediction dates back to 1994, when it was shown that an atom-thin Si sheet could be energetically viable in a buckled structure (Takeda & Shiraishi, 1994). However, it was not until 2012 that the initial compelling experimental proof of silicene emerged (Vogt et al., 2012). Since then, many fascinating properties and potential applications have been predicted for silicene, such as field-effect transistors for sensing and biosensing (Gablech et al., 2018), field-effect topological quantum transistors (Ezawa, 2015), negative differential-resistance devices (Chen et al., 2018), lithium-ion and sodium-ion batteries (Galashev et al., 2020; Wang et al., 2020), and biomedical field (Tao et al., 2019).

Despite the theoretical potential for various applications envisaged for silicene, its experimental synthesis remains a challenge (Masson & Prévot, 2023). Unlike graphene, which can be obtained through the mechanical exfoliation of graphite, silicene is typically derived via epitaxial growth on suitable substrates, showing a preference for ^{sp3} hybridization (Dávila & Lay, 2022). To date, it has been successfully synthesized on several substrates, predominantly metals, such as Ag(111) (Vogt et al., 2012), Ir(111) (Meng et al., 2013), Pb(111) (Stepniak-Dybala & Krawiec, 2019), Au(110) (Oughaddou et al., 2016), Au(111) (Stepniak-Dybala et al., 2019), ZrB2 (Fleurence et al., 2012), MoS_2 (Chiappe et al.), and graphite (De Crescenzi et al., 2016). The characterization of silicene is a complex task, necessitating various analytical approaches, including scanning tunneling microscopy, angle-resolved photoemission spectroscopy, and first principles calculations. Furthermore, the interpretation of these results can be significantly influenced by the substrate. Additionally, the structures obtained can assume numerous metastable

configurations depending on the substrate temperature and the flux of depositing Si atoms (Barboza et al., 2024). Consequently, many experimental findings are still subjects of debate (Van Bremen et al., 2017; Peng et al., 2018; Satta et al. 2018; Dávila et al., 2022).

Several theoretical studies have been conducted to investigate and better understand various properties and characteristics of silicene. These studies have explored electronic (Rojas-Cuervo et al., 2014; Huang et al., 2013; Tao et al., 2015; Kharadi et al., 2023), thermal (Liu et al., 2014; Gu & Yang, 2015), mechanical (Xu et al., 2014; Yang et al., 2014; Roman & Cranford, 2014), and optical properties (Das et al., 2015; Ye et al., 2014). However, most of these studies are conducted at 0 K and/or with a monolayer silicene (MS). Few-layer silicene (FLS) systems have been relatively overlooked in recent years, despite being significantly easier to synthesize than MS (Ipaves et al., 2022). Also, freestanding MS may face stability issues at room temperature without a substrate (Rouhi, 2017). Therefore, the existing works considering MS, regarding mechanical properties at room temperature, usually need to apply some form of constraining on the silicene's edges; otherwise, the system collapses during simulations. Although this approach is commonly applied in theoretical studies and may provide valuable information, it deviates from what one could expect from experiments.

Differing from MS, bilayer silicene (BS) has been predicted to maintain stability in a freestanding form at room temperature (Qian & Li, 2020). Also, BS exhibits versatile metallic or semiconducting behavior, depending on its morphology, making it highly appealing from a technological standpoint (Padilha et al., 2015). Surprisingly, the most stable stacking configuration of BS is demonstrated to be AA stacking (Liu et al., 2014; Padilha et al., 2015). In this arrangement, silicene loses its buckled structure, assuming a flat structural configuration (Qian & Li, 2020). Nevertheless, depending on the methodology employed, it is possible to encounter other types of structural configurations. Recent studies have identified AB stacking with a buckled configuration as the most stable, contradicting previous findings (Kharaldi et al., 2023). This

discrepancy may be attributed to the subtle differences in transition barriers between possible stacking configurations in silicene, suggesting its capacity for facile changes in stacking modes (Fu et al., 2014).

In the midst of the controversies surrounding silicene, a natural question that has arisen since its discovery is how the impact of doping on its properties would be. The logical candidates for doping silicene are Al and P, given their atomic radii closely align with that of Si, thereby minimizing lattice deformation. Numerous theoretical studies have investigated the electronic and optical properties of doped silicene (Lee et al., 2020; Li et al., 2023). Nevertheless, as of our current knowledge, simulations addressing the mechanical properties of doped bilayer silicene (DBS) on a large scale are notably absent from the literature.

These ongoing debates and controversies underline the challenges associated with the synthesis and characterization of silicene, emphasizing the need for further research to gain a deeper understanding of this intriguing material. Therefore, the objective of this work is to explore the mechanical properties of AA stacking BS doped with Al. For this purpose, we conducted molecular dynamics (MD) simulations utilizing a relatively recently developed potential from the literature for the Si-Al system (Starikov et al., 2020). The investigation delves into the impact of Al doping, ranging from 1% to 4%, on the mechanical properties of BS.

2 METHODOLOGY

The Large Scale Atomic/Molecular Massively Parallel Simulator (LAMMPS) (Thompson et al., 2022) serves as the platform for conducting the MD simulations, which is a commonly used code to study advanced materials (Andrade et al., 2021). Atomistic visualization and post-processing analyses are carried out using the Open Visualization Tool (OVITO) (Stukowski, 2009). The interatomic interactions involving Si-Si, Si-Al, and Al-Al pairs are defined using an angular-dependent potential (Starikov et al., 2020). This potential has exhibited high accuracy in

describing various phenomena within the Si-Al system, and has demonstrated good agreement with DFT calculations concerning numerous properties of pure Al, Si, and defective Si (Jouhari et al., 2023).

The creation of the BS structure utilizes the open-source program atomsk (Hirel, 2015), a widely employed software in computational materials science for generating, manipulating, and converting data files for atomic-scale simulations. The samples, both doped and pristine, possess dimensions of 280 Å x 280 Å, featuring an initial Si-Si bond length of 2.34 Å and a bond angle of 120°, as anticipated by theoretical studies (Chowdhury & Jana, 2016). An illustrative representation of a sample with 4% Al is depicted in Fig. 1. Doped specimens are derived from the pristine sample, with silicon atoms randomly substituted by aluminum atoms at specific percentages, namely, 1%, 2%, 3%, and 4%.

Figure 1 – Representative sample of bilayer silicene with 4% Al doping, showcasing the atomic structure where the purple and orange spheres represents Si and Al atoms, respectively. The zoomed area highlights the zigzag and armchair directions

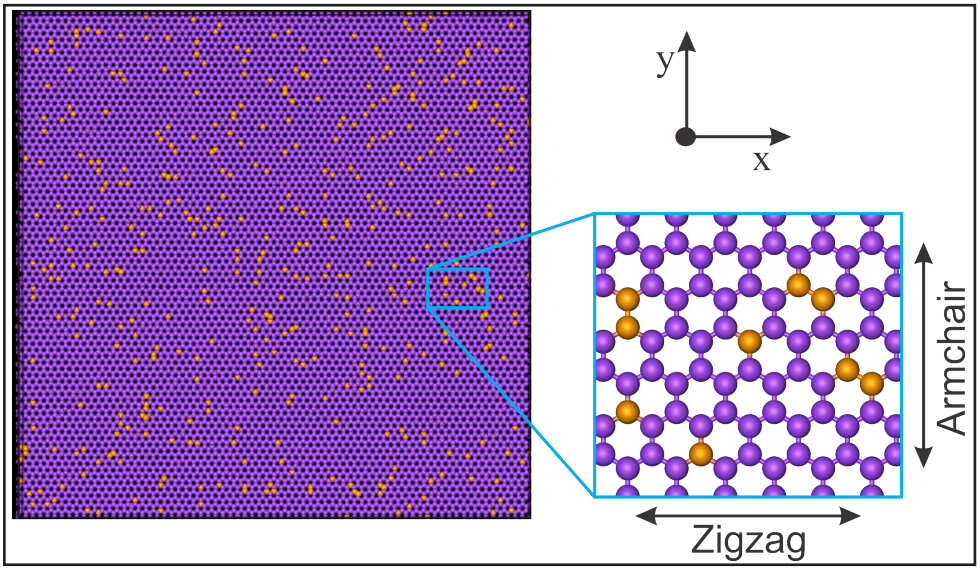

Source: Authors (2023)

During the simulation stages, periodic boundary conditions were applied along the x- and y-axis, while a fixed boundary have been established along the z-axis. The

Newton's equations of motion are solved using a time step of 1 femtosecond (fs) and the Velocity Verlet algorithm. Initially, the system's energy is minimized with the conjugate gradient method. Subsequently, initial velocities, corresponding to a temperature of 100 K, are assigned to the atoms with a Gaussian distribution. Then, the systems are heated over 20 ps until it reaches 300K, after which it is relaxed for an additional 20 ps. As show in Fig. 2, this duration proves adequate for achieving the necessary heating and relaxation period of the system. It is worth to mention that the temperature peak observed in Fig.2 during the initial stage is a normal occurrence in MD simulations and is merely an artifact resulting from the initial velocities of atoms.

Figure 2 – Temperature evolution during the simulation, illustrating the heating (red region) and relaxation (gray region) process of the BS system over a 40 ps timeframe, with 300 K as the final temperature. The initial temperature peak is a typical artifact observed in MD simulations due to the initial velocities of atoms

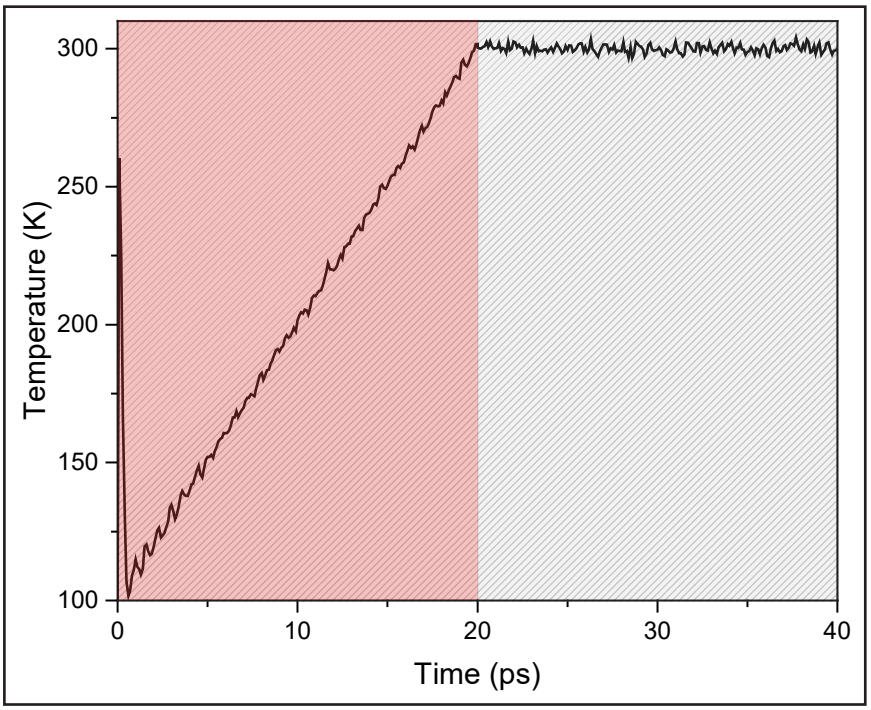

Source: Authors (2023)

Despite silicene being a 2D material, the stress results in this study are presented in bulk (3D) rather than 2D stresses. This transformation is accomplished by rescaling

the stress component, σ_{xx} or σ_{yy}, of the stress tensor, Eq. (1), using a factor of Z/δ_{BS}, where Z represents the vacuum dimension in z-direction and δ_{BS} is the thickness of the DBS. To compute the stress, the virial theorem is applied (Barboza et al., 2022):

$$\boldsymbol{\sigma} = -\frac{1}{V}\langle \sum_{i=1}^{N} m_i \boldsymbol{v_i} \times \boldsymbol{v_i} + \sum_{i=1}^{N} \boldsymbol{r_i} \times \boldsymbol{F_i} \rangle \quad (1)$$

where m_i, $\boldsymbol{v}_i$, $\boldsymbol{r}_i$, and $\boldsymbol{F}_i$ are the mass, instantaneous velocity, positions and the total force acting on the ith atom, respectively. The angle brackets denote an appropriate ensemble average over time of the virial stress, which is a requirement for it to be equivalent to the Cauchy stress (Subramaniyan & Sun, 2008). Therefore, in our simulations, a temporal average of the latest 100 time steps is used for the stress output at each time.

It is important to note that the thickness of the silicene structure cannot be easily determined experimentally, and due to its buckled structure, assigning a theoretical thickness is challenging, leading to ambiguity regarding the thickness of silicene (Roman & Crandord, 2014). In this context, we define the thickness of BS as δ_{BS}= h + 2δ, where h is the interlayer distance between two planar silicene layers, measuring 2.41 Å (Fu et al., 2014), and δ is the thickness equivalent to the crystalline thickness of silicon, 1.34 Å (Roman & Cranford, 2014). Thus, the δ_{BS} used in this work is 5.1 Å.

Lastly, uniaxial tensile tests are conducted along both the zigzag (ZZ) and armchair (AC) directions at a strain rate of 10^{10} s^{-1}. It is worth noting that, despite the random doping, both the AC and ZZ tensile tests for a given doping concentration utilize the same sample to mitigate stochastic effects.

3 RESULTS

The DBS samples, with Al concentrations ranging from 1% to 4%, undergo uniaxial tensile tests, and the resulting stress-strain responses of the systems

are recorded. Figure 3(a) and (b) show the obtained curves at 300 K and a strain rate of 10^{10} s^{-1} for AC and ZZ directions, respectively. One can note that the stress-strain relationship is linear at lower levels of strain. However, after approximately 0.025 (0.020) strain, the stress begins to rises nonlinearly until reaching $\varepsilon \approx 0.13$ (0.11), after which it resumes a linear relation until reaching the ultimate tensile strength (UTS) and ultimately fails catastrophically for ZZ and (AC) directions. It is intriguing to observe that this pattern persists regardless of the doping level, as even the pristine BS exhibits a similar behavior. Controversial results exist in the literature regarding the stress-strain curve pattern of silicene. While some studies with pristine MS and BS align with the present work's trend (Roman & Cranford, 2014), others have obtained a curve with a single linear region from the beginning until fracture (Nahid et al., 2018).

As seen in Table 1, there is a considerable dispersion in results regarding the mechanical properties of BS, likely stemming from differences in methodology across studies. Three main reasons could account for this variability. Firstly, the thickness of BS applied in some works is not adequately explained, hindering the possibility of rescaling to a 2D stress and applying the thickness used in this study for comparison. Secondly, variations in the applied strain rate are known to induce changes in stress and strain values. Thirdly, and arguably most significantly, discrepancies arise from the use of different interatomic potentials. The ReaxFF-type potential employed in Qian & Li, 2020, parameterized in 2013 for the interaction between oxygen and silica, may not be the most suitable for studying the mechanical properties of BS. The hybrid potential in Rouhi et al., 2019, combining Tersoff for intralayer Si-Si interactions and Lennard-Jones for interlayer interactions, is recognized for yielding less accurate results. Finally, the EDIP-type potential in Castillo et al., 2018, as demonstrated to be inadequate for simulating MS by Maździarz, 2023, can be expected to yield even less favorable results for BS.

Table 1 – Comparative overview of mechanical properties of pristine BS reported in various studies, with focus on Young's modulus (E), ultimate tensile stress (UTS), and ultimate strain (US)

	E **(GPa)**	**UTS (GPa)**	**US**
AC	139.5[a]	39.5[a]	0.32[a]
	106.6[b]	18.6[b]	0.18[b]
	172.3[c]	14.6[c]	0.13[c]
	187.8[d]	18.44[d]	0.147[d]
ZZ	127.3[a]	27.0[a]	0.25[a]
	106.5[b]	22.5[b]	0.33[b]
	185.0[d]	25.86[d]	0.190[d]

[a] Rouhi (2019)

[b] Qian (2020)

[c] Maździarz (2023)

[d] This work

Both loading directions show an overall reduction in stress and strain, as expected, given that a similar pattern is observed for ML as well (Nahid et al., 2018). Another insight from Fig. 3 is that with an increase in the concentration of Al, the area under the stress-strain curves gradually decreases. Consequently, the total energy density absorbed by the material until fracture, known as fracture toughness, diminishes with the increasing concentration of Al doping. Additionally, the mechanical characteristics of DBS persist in exhibiting the inherent anisotropies typical of planar honeycomb structures (Rahman et al., 2020). The variations in properties along the AC and ZZ directions are notably influenced by the bond angle and bond orientation concerning the applied load.

Figure 3(c) and (d) display the ultimate tensile stress (UTS) and ultimate strain (US) with varying percentages of Al. The impact of Al doping on the mechanical properties of DBS becomes more evident in this figure. It is observed that with an increase in Al concentration, both UTS and US gradually decrease. Specifically, with 4% aluminum doping, the UTS and US for ZZ (AC) direction are decreased by 35% (21%) and 16% (12%), respectively. Consequently, the mechanical properties of DBS experience a

significant decline with the increasing concentration of Al. This decline can be attributed to diminished bond strength, lattice deformation, and void formation resulting from aluminum doping, as previously observed in other 2D materials (Mortazavi & Ahzi, 2012).

Figure 3 – Stress-strain curves of DBS at 300 K for different percentage of Al doping along (a) ZZ and (b) AC directions. Variations of (c) UTS and (d) US with Al concentration

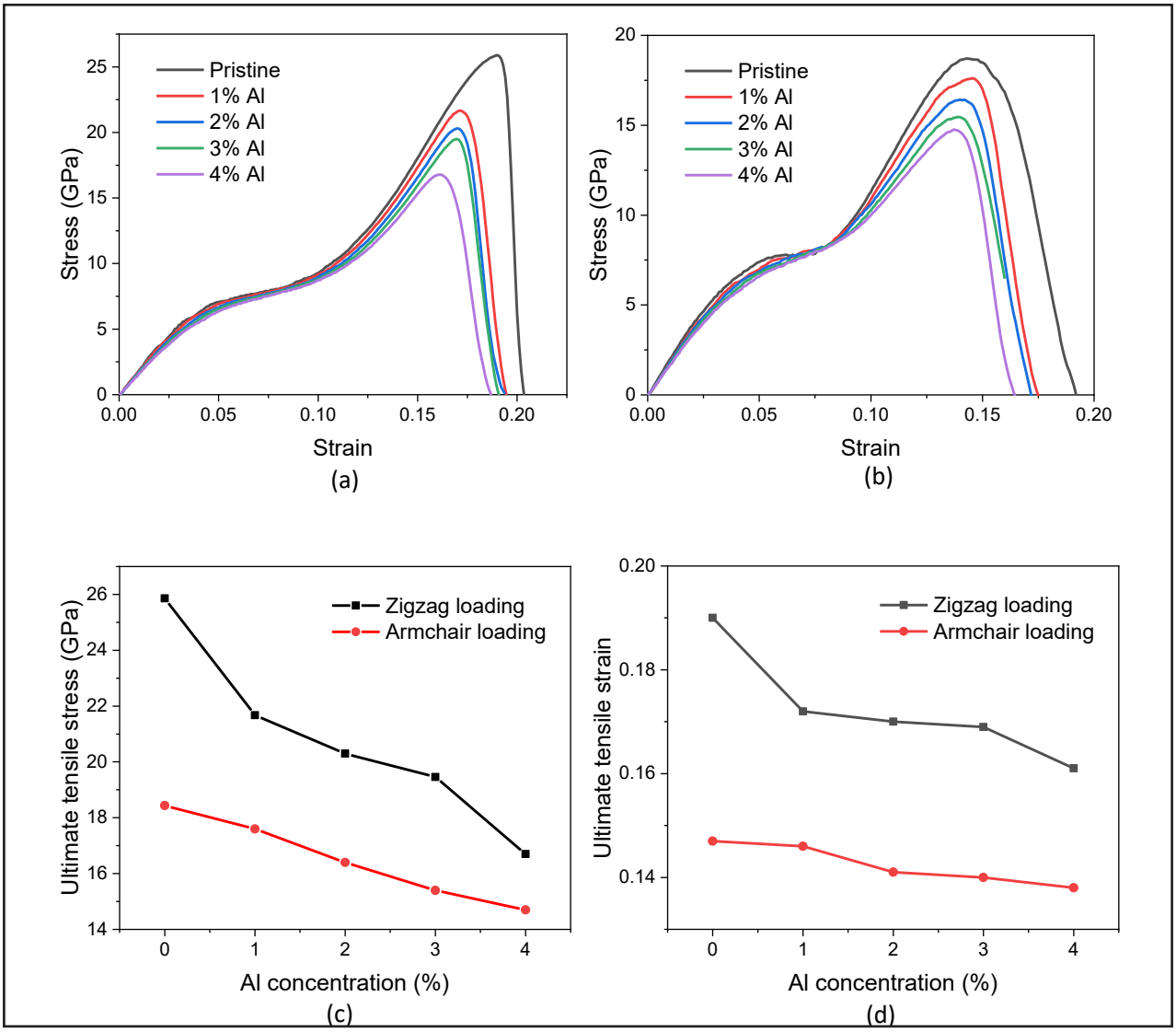

Source: Authors (2023)

The Si-Si bond energy is higher at 327 kJ/mol compared to the Si-Al bond energy at 251 kJ/mol (Dean, 1999). Consequently, breaking the Al-Si bond requires less strain than breaking the Si-Si bond. This is particularly relevant in the case of 4% DBS, where

a substantial amount of Si-Al bonds is present, resulting in the lowest UTS and US. Moreover, the introduction of Al into DBS induces out-of-plane and lattice deformation of the silicene lattice, as illustrated in Fig. 4. In Figure 4(a), a specific region is highlighted where some Al atoms are concentrated, including a sequence of three bonded Al atoms. Figure 4(b) represents the same region, with the atoms colored according to their respective potential energy, revealing that the lattice nearby Al atoms undergoes deformation, indicated by their higher energy state. This deformation is particularly noticeable when there is a relatively high concentration of doping elements in a small area. These areas are more likely to initiate voids at lower stress and strains compared to a pristine BS.

Figure 4 – Deformation of the silicene lattice in DBS with 4% Al. (a) Highlights a specific region with concentrated Al atoms, including a sequence of three bonded Al atoms. (b) Represents the same region with atoms colored according to their respective potential energy, illustrating lattice deformation around Al atoms. The potential energy increases from color blue to red

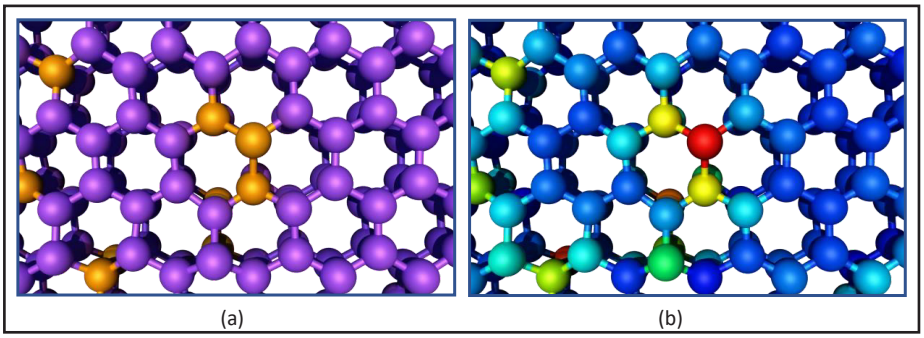

Source: Authors (2023)

Figure 5 illustrates the fracture process, revealing that shortly after the initial rupture of the Si-Al bond, additional debonding occurs among the nearest pair of atoms as the strain continues to rise. Ultimately, this process leads to the specimen undergoing complete fracture. It can be inferred that the fracture of DBS initiates at locations where the concentration of Al atoms is highest within the system. Furthermore, it is evident from Figure 3 that the mechanical properties of DBS deteriorate, irrespective of chirality, with an increase in the concentration of Al within the DBS structure.

Figure 5 – Fracture process in doped bilayer silicene (DBS) with 4% Al doping. The illustration demonstrates that after the (a) initial rupture of the Si-Al bond, (b) additional debonding occurs among the nearest pair of atoms as the strain increases, ultimately leading to (c-d) complete fracture

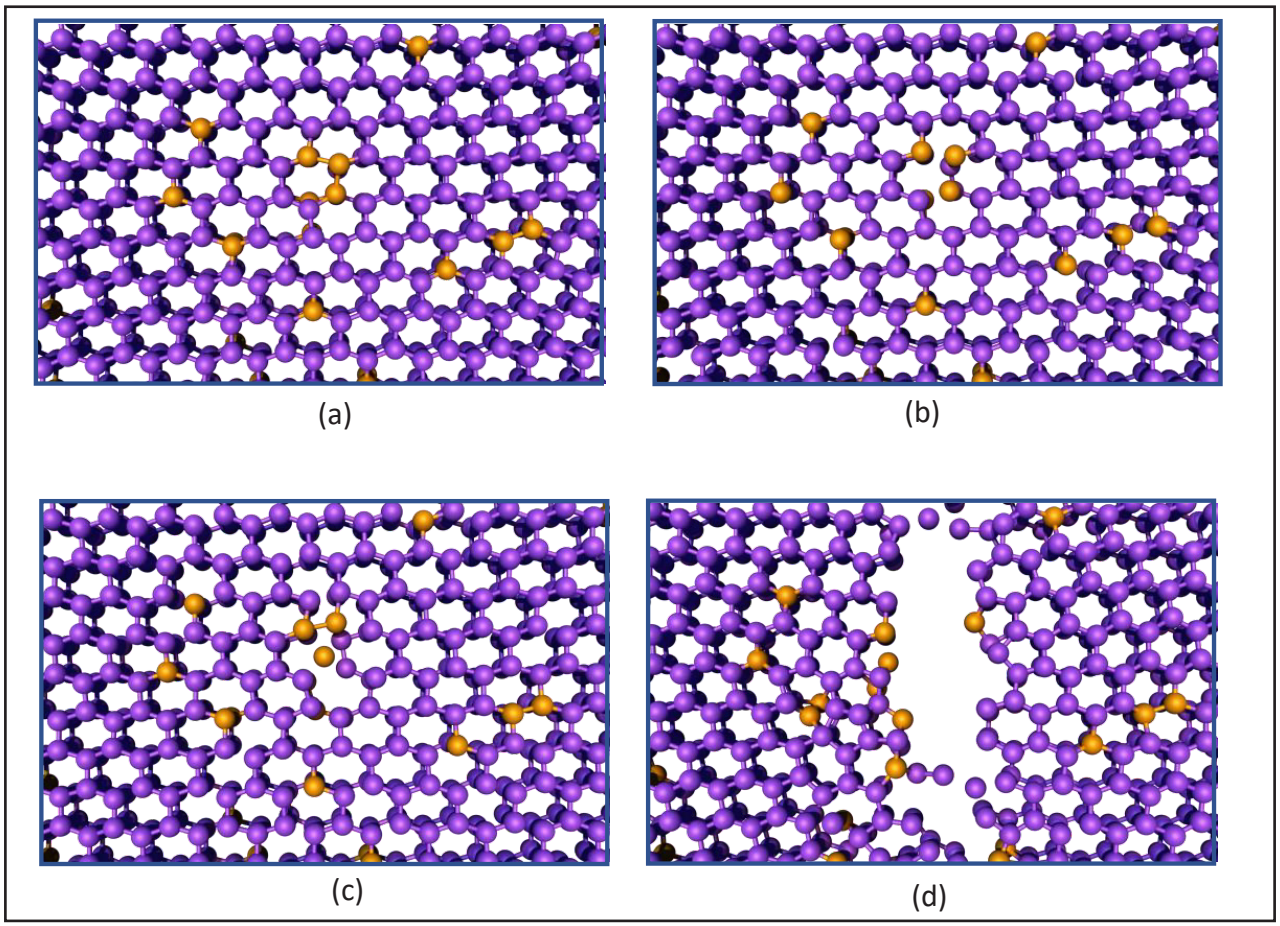

Source: Authors (2023)

Young's modulus (E) was determined by fitting the curve with linear regression, focusing on the initial linear region (strain values between 0% and 2%) of the stress-strain curve. The results in Table 2 suggest an inverse relationship of E with the concentration of Al doping. It has been observed that 4% Al reduces E by approximately 15% and 12% for ZZ and AC directions, respectively. Hence, the DBS in the ZZ direction is more sensitive to Al doping concerning Young's modulus. Similar reductions in E caused by doping have been noted in other 2D materials, such as nitrogen or silicon-doped graphene Mortazavi et al., 2012).

Table 2 – Young's modulus values for DBS under varying concentrations of Al doping, indicating an inverse relationship between E and the concentration of Al

	E (GPa)				
Al concentration	0%	1%	2%	3%	4%
Armchair loading	187.8	184.6	178.7	171.9	164.7
Zigzag loading	185.0	180.2	171.6	164.7	158.0

Source: Authors (2023)

4 CONCLUSIONS

This study explored the mechanical properties of Al-doped bilayer silicene through molecular dynamics simulations. The findings underscore the complex interplay of defect dynamics, doping effects, and loading direction in shaping the mechanical behavior of DBS.

Our investigation reveals that the introduction of Al into the BS structure adversely affects its mechanical properties. Increasing Al concentrations result in a gradual decline in both ultimate tensile strength (UTS) and strain (US). The ZZ loading was shown to be more sensitive to Al doping, with a reduction in stress and strain of 35% and 16%, respectively. Following this trend, the Young's modulus also exhibited a significant reduction with increasing Al doping.

The rupture of DBS initiates with the breakage of Al-Si bonds, which consequently leads to further debonding in the nearby lattice leading to a fragile fracture.

ACKNOWLEDGEMENTS

The authors thank the financial support from the Fundação de Amparo à Pesquisa do Estado do Rio de Janeiro (FAPERJ) – Processo SEI-260003/002235/2022 and SEI-260003/001582/2022 –, Conselho Nacional de Desenvolvimento Científico e Tecnológico (CNPq), and Coordenação de Aperfeiçoamento de Pessoal de Nível Superior – Brasil (CAPES) – Finance Code 001.

REFERENCES

Andrade, J. S., Bastos, I. N., Aliaga, L. C. R. (2021). Determinação das características estruturais e mecânicas da liga de alta entropia Hf-Nb-Ta-Zr. VETOR - Revista De Ciências Exatas E Engenharias, 30(2), 22–32. https://doi.org/10.14295/vetor.v30i2.13090.

Barboza, A. M., Aliaga, L. C. R., Faria, D., Bastos, I. N. (2022). Bilayer graphene kirigami, Carbon Trends, 9, 100227. https://doi.org/10.1016/j.cartre.2022.100227.

Barboza, A. M., Silva-Santos, J. A., Aliaga, L. C. R., Bastos, I. N., Faria, D. (2024). Silicene growth mechanisms on Au(111) and Au(110) substrates, Nanotechnology, 35, 165602. https://doi.org/10.1088/1361-6528/ad1aff.

Castillo, M. R. C., Meza, M. A. R., Montes, L. M. (2018). Mechanical response of bilayer silicene nanoribbons under uniaxial tension. RSC Advances, 8, 10785–10793. https://doi.org/10.1039/C7RA12482A.

Chen, C.-H., Li, W.-W., Chang, Y.-M., Lin, C.Y. et al. (2018). Negative-Differential-Resistance Devices Achieved by Band-Structure Engineering in Silicene under Periodic Potentials. Physical Review Applied, 10, 044047. https://doi.org/10.1103/PhysRevApplied.10.044047.

Chiappe, D., Scalise, E., Cinquanta, E., Grazianetti, C. et al. (2014). Two-Dimensional Si Nanosheets with Local Hexagonal Structure on a MoS2 Surface. Advanced Materials, 26, 2096–2101. https://doi.org/10.1002/adma.201304783.

Chowdhury, S., Jana, D. (2016). A theoretical review on electronic, magnetic and optical properties of silicene. Reports on Progress in Physics, 79, 126501. https://doi.org/10.1088/0034-4885/79/12/126501.

Dávila, M. E., Lay, G. L. (2022). Silicene: Genesis, remarkable discoveries, and legacy. Materials today advances, 16, 100312. https://doi.org/10.1016/j.mtadv.2022.100312.

Das, R., Chowdhury, S., Majumdar, A., Jana, D. (2015). Optical properties of P and Al doped silicene: a first principles study. RSC Advances, 5, 41–50. https://doi.org/10.1039/C4RA07976K.

De Crescenzi, M., Berbezier, I., Scarselli, M., Castrucci, P. et al. (2016). Formation of Silicene Nanosheets on Graphite. ACS Nano, 10, 11163–11171. https://doi.org/10.1021/acsnano.6b06198.

Dean, J.A. (1999). Lange's Handbook of Chemistry. 15th Edition, McGraw-Hill, Inc., New York, St. Louis, San Francisco.

Ezawa, M. (2015). Monolayer Topological Insulators: Silicene, Germanene, and Stanene. Journal of the Physical Society of Japan, 84, 121003. https://doi.org/10.7566/JPSJ.84.121003.

Fleurence, A., Friedlein, R., Ozaki, T., Kawai, H. et al. (2012). Experimental Evidence for Epitaxial Silicene on Diboride Thin Films. Physical Review Letters, 108, 245501. https://doi.org/10.1103/PhysRevLett.108.245501.

Fu, H., Zhang, J., Ding, Z., Li, H. et al. (2014). Stacking-dependent electronic structure of bilayer silicene. Applied Physics Letters, 104 (13), 131904. https://doi.org/10.1063/1.4870534.

Gablech, I., Pekárek, J., Klempa, J., Svatoš, V. et al. (2018). Monoelemental 2D materials-based field effect transistors for sensing and biosensing: Phosphorene, antimonene, arsenene, silicene, and germanene go beyond graphene. TrAC Trends in Analytical Chemistry, 105, 251–262. https://doi.org/10.1016/j.trac.2018.05.008.

Galashev, A. Y., Suzdaltsev, A. V., Ivanichkina, K. A. (2020). Design of the high performance microbattery with silicene anode. Materials Science and Engineering B, 261, 114718. https://doi.org/10.1016/j.mseb.2020.114718.

Gu X., Yang, R. (2015). First-principles prediction of phononic thermal conductivity of silicene: a comparison with graphene. Journal of Applied Physics, 117, 025102(1). https://doi.org/10.1063/1.4905540.

Hirel, P. (2015). Atomsk: A tool for manipulating and converting atomic data files, Computer Physics Communications, 197, 212–219. https://doi.org/10.1016/j.cpc.2015.07.012.

Huang, S., Kang, W., Yang, L. (2013). Electronic structure and quasiparticle bandgap of silicene structures. Applied Physics Letters, 102, 133106(1). https://doi.org/10.1063/1.4801309.

Ipaves, B., Justo, J. F., Assali, L. V. C. (2022). Functionalized few-layer silicene nanosheets: stability, elastic, structural, and electronic properties. Physical Chemistry Chemical Physics, 24, 8705–8715. https://doi.org/10.1039/D1CP05867C.

Jouhari, C., Liu, Y., Dickel, D. (2023). Phase-Field Modeling of Aluminum Foam Based on Molecular Dynamics Simulations. In: TMS 2023 152nd Annual Meeting & Exhibition Supplemental Proceedings, 632–641.

Kharadi, M. A., Mittal, S., Saha, J. (2023). Structural, electronic and optical properties of fluorinated bilayer silicene. Optical Materials, 136, 113418. https://doi.org/10.1016/j.optmat.2022.113418.

Lee, K. W., Lee, C. E. (2020). Strain and doping effects on the antiferromagnetism of AB-stacked bilayer silicene. Physica B: Condensed Matter, 577, 411816. https://doi.org/10.1016/j.physb.2019.411816.

Li, W. Z., He, Y., Mao, Y., Xiong, K. (2023). Tuning of magnetic, electronic and electrolytic water properties of silicene supported precious-metal by non-metal doping and vacancy defect, FlatChem, 38, 100486. https://doi.org/10.1021/acsomega.2c03388.

Liu, B., Reddy, C. D., Jiang, J., Zhu, H. et al. (2014). Thermal conductivity of silicene nanosheets and the effect of isotopic doping. Applied Physics Letters, 47, 165301(1). https://doi.org/10.1088/0022-3727/47/16/165301.

Masson, L., Prévot, G. (2023). Epitaxial growth and structural properties of silicene and other 2D allotropes of Si. Nanoscale Advances, 5, 1574. DOI https://doi.org/10.1039/D2NA00808D.

Maździarz, M. (2023). Transferability of interatomic potentials for silicene. Beilstein Journal of Nanotechnology, 14, 574–585. https://doi.org/10.3762/bjnano.14.48.

Meng, L., Wang, Y., Zhang, L., Du, S. et al. (2013). Buckled Silicene Formation on Ir(111). Nano Letters, 13, 685–690. https://doi.org/10.1021/nl304347w.

Mortazavi, B., Ahzi, S. (2012). Molecular dynamics study on the thermal conductivity and mechanical properties of boron doped graphene. Solid State Communications, 152, 15, 1503–1507. https://doi.org/10.1016/j.ssc.2012.04.048.

Mortazavi, B., Ahzi, S., Toniazzo, V., Rémond, Y. (2012). Nitrogen doping and vacancy effects on the mechanical properties of graphene: A molecular dynamics study. Physics Letters A, 376, Issues 12–13, 1146–1153. https://doi.org/10.1016/j.physleta.2011.11.034.

Nahid, S. M., Nahian, S., Motalab, M., Rakib, T. et al. (2018). Tuning the mechanical properties of silicene nanosheet by auxiliary cracks: a molecular dynamics study. RSC Advances, 8, 30354–30365. https://doi.org/10.1039/C8RA04728F.

Oughaddou, H., Enriquez, H., Tchalala, M. R., Bendounan, A. et al. (2016). Silicene: Structure, Properties and Applications; Spencer, M. J., Morishita, T., Eds., Springer International Publishing: Cham, 167–181. https://doi.org/10.1007/978-3-319-28344-9_8.

Padilha, J. E., Pontes, R. B. (2015). Free-Standing Bilayer Silicene: The Effect of Stacking Order on the Structural, Electronic, and Transport Properties. Journal of Physical Chemistry C, 119 (7), 3818–3825. https://doi.org/10.1021/jp512489m.

Peng, W., Xu, T., Diener, P., Biadala, L. et al. (2018). Resolving the Controversial Existence of Silicene and Germanene Nanosheets Grown on Graphite. ACS Nano, 12, 4754–4760. https://doi.org/10.1021/acsnano.8b01467.

Qian, C., Li, Z. (2020). Multilayer silicene: Structure, electronics, and mechanical property, Computational Materials Science, 172, 109354. https://doi.org/10.1016/j.commatsci.2019.109354.

Rahman, Md. H., Mitra, S., Motalaba, M., Bose, P. (2020). Investigation on the mechanical properties and fracture phenomenon of silicon doped graphene by molecular dynamics simulation. RSC Advances, 10, 31318–31332. https://doi.org/10.1039/D0RA06085B.

Rojas-Cuervo, A. M., Fonseca-Romero K. M., Rey-González, R. R. (2014). Anisotropic Dirac cones in monoatomic hexagonal lattices a DFT study. The European Physical Journal B, 87, 67. https://doi.org/10.1140/epjb/e2014-40894-9.

Roman, R. E., Cranford, S. W. (2014). Mechanical properties of silicene. Computational Materials Science, 82, 50–55. https://doi.org/10.1016/j.commatsci.2013.09.030.

Rouhi, S. (2017). Fracture behavior of hydrogen-functionalized silicene nanosheets by molecular dynamics simulations. Computational Materials Science, 131, 275–285. https://doi.org/10.1016/j.commatsci.2017.02.007.

Rouhi, S., Pourmirzaagha, H., Farzin, A. et al. (2019). Predicting the mechanical properties of multi-layered silicene by molecular dynamics simulations. Materials Research Express, 6, 085004. https://doi.org/10.1088/2053-1591/ab1b81.

Satta, M., Lacovig, P., Apostol, N., Dalmiglio, M. et al. (2018). The adsorption of silicon on an iridium surface ruling out silicene growth. Nanoscale, 10, 7085–7094. https://doi.org/10.1039/C8NR00648B.

Starikov, S., Gordeev, I., Lysogorskiy, Y., Kolotova, L. et al. (2020). Optimized interatomic potential for study of structure and phase transitions in Si-Au and Si-Al systems. Computational Materials Science, 184, 109891. https://doi.org/10.1016/j.commatsci.2020.109891.

Stepniak-Dybala, A., Krawiec, M. (2019). Formation of Silicene on Ultrathin Pb(111) Films. Journal of Physical Chemistry C, 123, 17019–17025. https://doi.org/10.1021/acs.jpcc.9b04343.

Stepniak-Dybala, A., Dyniec, P., Kopciuszyski, M., Zdyb, R. et al. (2019). Planar Silicene: A New Silicon Allotrope Epitaxially Grown by Segregation. Advanced Functional Materials, 29, 1906053. https://doi.org/10.1002/adfm.201906053.

Stukowski, A. Visualization and analysis of atomistic simulation data with OVITO–the Open Visualization Tool. (2009). Modelling and Simulation in Materials Science and Engineering, 18, 015012. https://doi.org/10.1088/0965-0393/18/1/015012.

Subramaniyan, A. K., Sun, C. T. (2008). Continuum interpretation of virial stress in molecular simulations. International Journal of Solids and Structures, 45, 4340–4346. https://doi.org/10.1016/j.ijsolstr.2008.03.016.

Takeda, K., Shiraishi, K. (1994). Theoretical possibility of stage corrugation in Si and Ge analogs of graphite. Physical Review B, 50, 14916–14922. https://doi.org/10.1103/PhysRevB.50.14916.

Tao, L., Cinquanta, E., Chiappe, D., Grazianetti, C., Fanciulli, M. et al. (2015). Silicene field-effect transistors operating at room temperature. Nature Nanotech, 10, 227–231. https://doi.org/10.1038/nnano.2014.325.

Tao, W., Kong, N., Ji, X., Zhang, Y. et al. (2019). Emerging two-dimensional monoelemental materials (Xenes) for biomedical applications. Chemical Society Reviews, 48, 2891–2912. https://doi.org/10.1039/C8CS00823J.

Thompson, A. P., Aktulga, H. M., Berger, R., Bolintineanu, D. S. et al. (2022). LAMMPS - a flexible simulation tool for particle-based materials modeling at the atomic, meso, and continuum scales. Computer Physics Communications, 271, 108171. https://doi.org/10.1016/j.cpc.2021.108171.

Van Bremen, R.; Yao, Q., Banerjee, S., Cakir, D., Oncel, N. et al. (2017). Intercalation of Si between MoS(2) layers. Beilstein Journal of Nanotechnology, 8, 1952–1960. https://doi.org/10.3762/bjnano.8.196.

Vogt, P., De Padova, P., Quaresima, C., Avila, J. et al. (2012). Silicene: Compelling Experimental Evidence for Graphene like Two-Dimensional Silicon. Physical Review Letters, 108, 155501. https://doi.org/10.1103/PhysRevLett.108.155501.

Xu, P., Yu, Z., Yang, C., Lu, P. et al (2014). Comparative study on the nonlinear properties of bilayer graphene and silicene under tension. Super Lattices and Microstructures, 75, 647–656. https://doi.org/10.1016/j.spmi.2014.08.022.

Wang, T., Li, C., Xia, C., Yin, L. et al. (2020). Silicene/BN vdW heterostructure as an ultrafast ion diffusion anode material for Na-ion battery. Physica E: Low-dimensional Systems and Nanostructures, 122, 114146. https://doi.org/10.1016/j.physe.2020.114146.

Yang, C., Yu, Z., Lu, P., Liu, Y. et al. (2014). Phonon instability and ideal strength of silicene under tension. Computational Materials Science, 95, 420–428. https://doi.org/10.1016/j.commatsci.2014.07.046.

Ye X. S., Shao Z. G., Zhao H., Yang L. et al. (2014). Electronic and optical properties of silicene nanomeshes. RSC Advances, 4, 37998. https://doi.org/10.1039/C4RA03942D.

Authorship contributions

1 – Bryan Angel Leite dos Santos

Universidade do Estado do Rio de Janeiro - Mechanical engineering student
https://orcid.org/0009-0003-1709-3530 - bryan.santos@grad.iprj.uerj.br
Contribution: Investigation, Methodology, Writing – original draft, Visualization

2 – Alexandre Melhorance Barboza

Universidade do Estado do Rio de Janeiro - PhD in computational modeling
https://orcid.org/0000-0001-6416-2138 - abarboza@iprj.uerj.br
Contribution: Investigation, Conceptualization, Supervision, Project administration, Methodology, Writing – review & editing, Validation

3 – Luis César Rodríguez Aliaga

Universidade do Estado do Rio de Janeiro - PhD in Materials Science
https://orcid.org/0000-0002-5397-674X - aliaga@iprj.uerj.br
Contribution: Methodology, Formal analysis, Writing – review & editing

4 – Ivan Napoleão Bastos

Universidade do Estado do Rio de Janeiro - PhD in Metallurgical and Materials Engineering
https://orcid.org/0000-0001-7611-300X - inbastos@iprj.uerj.br
Contribution: Writing – review & editing, Resources, Funding acquisition

How to quote this article

Santos, B. A. L. dos, Barboza, A. M., Aliaga, L. C. R., & Bastos, I. N. (2024). Influence of aluminum doping on the mechanical properties of bilayer silicene. *Ciência e Natura,* 46, spe. 1, e87036. https://doi.org/10.5902/2179460X87036.